

# Selective and Collective Actuation in Active Solids

P. Baconnier<sup>1</sup>, D. Shohat<sup>1,2</sup>, C. Hernandéz<sup>3,4</sup>, C. Coulais<sup>5</sup>, V. Démery<sup>1,6</sup>, G. Düring<sup>3,4</sup>, O. Dauchot<sup>1,\*</sup>

Active solids consist of elastically coupled out-of-equilibrium units performing work<sup>1–13</sup>. They are central to autonomous processes, such as locomotion, self-oscillations and rectification, in biological systems<sup>14–25</sup>, designer materials<sup>26</sup> and robotics<sup>27–31</sup>. Yet, the feedback mechanism between elastic and active forces, and the possible emergence of collective behaviours in a mechanically stable elastic solid remains elusive. Here we introduce a minimal realization of an active elastic solid, in which we characterize the emergence of selective and collective actuation and fully map out the interplay between activity, elasticity and geometry. Polar active agents exert forces on the nodes of a two dimensional elastic lattice. The resulting displacement field nonlinearly reorients the active agents. For large enough coupling, a collective oscillation of the lattice nodes around their equilibrium position emerges. Only a few elastic modes are actuated and, crucially, they are not necessarily the lowest energy ones. Combining experiments with the numerical and theoretical analysis of an agents model, we unveil the bifurcation scenario and the selection mechanism by which the collective actuation takes place. Our findings may provide a new mechanism for oscillatory dynamics in biological tissues<sup>15</sup> and specifically confluent cell monolayers<sup>14,19,24</sup>. The present selection mechanism may also be advantageous in providing meta-materials<sup>32</sup>, with bona fide autonomy<sup>33</sup>.

Active solids<sup>1–13</sup> combine the central properties of simple elastic solids and active liquids<sup>34–39</sup> (Fig. 1-a). On one hand the positional degrees of freedom of their constituting units have a well-defined reference state. On the other hand activity endows these units with an additional free degree of freedom in the form of polar, or dipolar, active forces. In active liquids, aligning interactions between these forces lead to collective motion. In active solids these active forces deform the elastic matrix, and induce a strain field, which depends on the forces configuration. This strain tensor will in turn reorient the forces. This generic nonlinear elasto-active

feedback, a typical realization of which is the contact inhibition locomotion (CIL) of cells<sup>14,19</sup>, opens the path towards spontaneous collective excitations of the solid, which we shall call collective actuation. In this work we propose a minimal experimental setting and numerical model, in which we unveil the modal selectivity of collective actuation and its underlying principles.

We consider crystalline lattices with, at the center of each node, an active particle with a fluctuating orientation (Fig. 1-b and Methods). Each node has a well defined reference position, but will be displaced by the

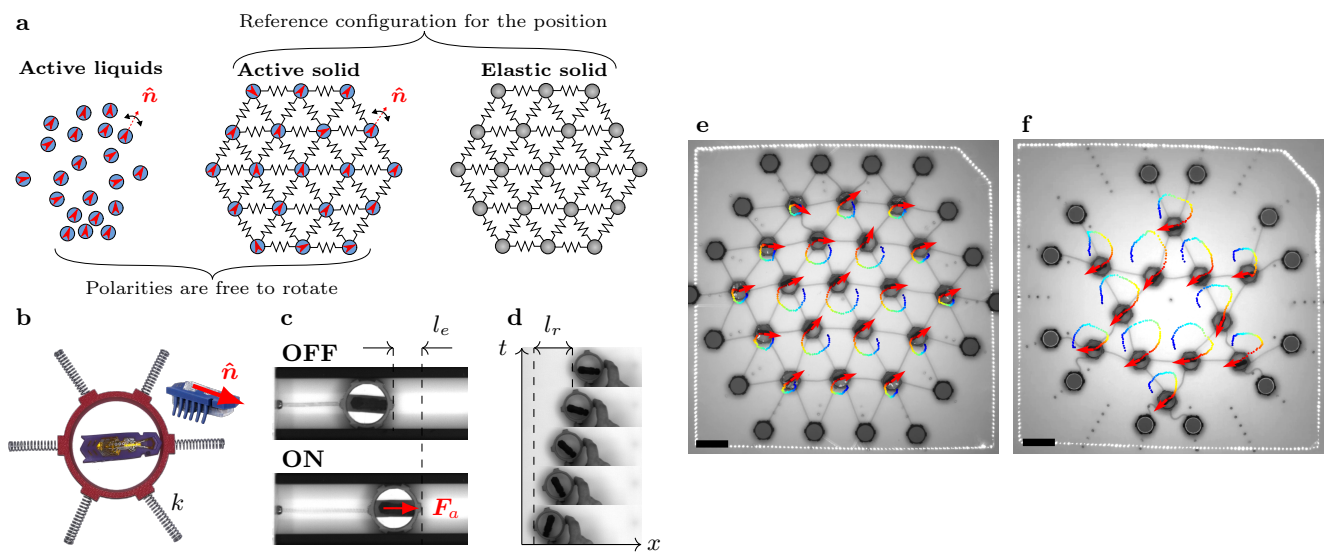


**FIG. 1. Design principle and Collective Actuation.** **a**, Active solids have positional degrees of freedom with a reference state, and a free to rotate polarity vector in the direction of the active force. **b**, Active unit : a hexbug is trapped in a 3d printed cylinder. **c**, The active component, here confined in a linear track and attached to a spring of stiffness  $k$ , produces an active force of amplitude  $F_0$  in the direction of the polarity  $\hat{\mathbf{n}}$  and elongates the spring by a length  $l_e = F_0/k$ . **d**, The hexbug aligns toward the displacement, here imposed manually, of the cylinder (see Supplementary Information for a quantitative measure of the reorientation length  $l_r$ ). **e,f**, When embedded in a 2d triangular (e) or kagome (f) elastic lattice, pinned at its edges, the nonlinear coupling drives the system towards collective actuation dynamics (red arrows: polarities  $\hat{\mathbf{n}}_i$ ; trajectories color coded from blue to red by increasing time; scale bars: 10 cm).

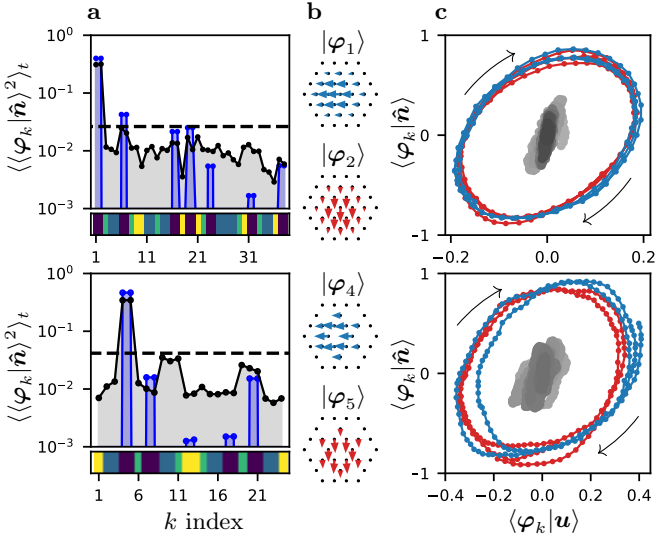


**FIG. 2. Selectivity of the actuated modes** **a**, Spectral decomposition of dynamics on the normal modes of the (top) triangular and (bottom) kagome lattices, sorted by order of growing energies (grey: experiments; blue: numerics). The horizontal dashed lines indicate equipartition. The bottom color bars codes for the symmetry class of the modes (Supplementary Information section 6). **b**, Sketch of the two most excited modes, which are not necessarily the lowest energy ones. **c**, Normal modes components of the active forces as a function of the normal modes components of the displacements (blue/red : projection on  $|\varphi_{1/2}\rangle$ , grey : other modes).

active particles (Fig. 1-c). In contrast, the polarization of each particle is free to rotate and reorients towards its displacement (Fig. 1-d, Supplementary Information section 2.2.2 and Movie 1). This nonlinear feedback between deformations and polarizations is characterized by two length-scales: (i) the typical elastic deformation caused by active forces  $l_e$  (Fig. 1-b) and (ii) the reorientation length  $l_r$  (Fig. 1-c). If not hold, such an active solid adopts a translational and/or rotational rigid body motion (see Supplementary Information section 1, Movies 2 and 3), as also observed in theoretical models<sup>3,5,16</sup>. Here we are interested in stable elastic solids, with no zero-modes. We therefore explore the emergence of collective dynamics in a triangular (Fig. 1-d) and a kagome (Fig. 1-e) lattice, pinned at their edges. We observe that all the lattice nodes spontaneously break chiral symmetry and rotate around their equilibrium position in a collective steady state (Fig. 1-d,e and Movies 5,8). This dynamical and chiral phase is reminiscent of oscillations in biological tissues<sup>15,24</sup>. It is clearly different from collective dynamics in active fluids<sup>35,36</sup> and rigid body motion in active solids<sup>3,5,9</sup>.

In the remainder of the manuscript, we unveil the modal selectivity of this collective actuation and develop the key elements of its understanding. To do so, we complement the experiments with numerical simulations (Methods) of harmonically coupled self-aligning active particles<sup>40</sup>. In the over-damped, harmonic and noiseless limit, the model reads:

$$\dot{\mathbf{u}}_i = \pi \hat{\mathbf{n}}_i - \mathbb{M}_{ij} \mathbf{u}_j \quad (1.1)$$

$$\dot{\mathbf{n}}_i = -(\hat{\mathbf{n}}_i \times \mathbb{M}_{ij} \mathbf{u}_j) \times \hat{\mathbf{n}}_i, \quad (1.2)$$

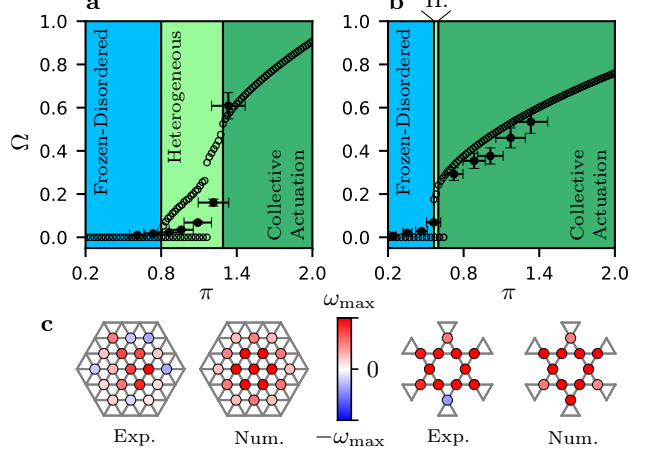


**FIG. 3. Transition to collective actuation in the triangular (left) and kagome (right) lattices.** **a,b**, Average oscillation frequency  $\Omega$  as a function of  $\pi$  (plain bullets: experiments; open circles: numerics). Background colors code for the dynamical regime (light blue: frozen and disordered; light green: heterogeneous (H); dark green: collective actuation). Triangular:  $\pi_{FD} = 0.800$ ,  $\pi_{CA} = 1.29$ ; kagome:  $\pi_{FD} = 0.564$ ,  $\pi_{CA} = 0.600$ . **c**, Individual oscillation frequencies  $\omega_i$  illustrating the coexistence dynamics in experiments and numerical simulations; (triangular lattice:  $\pi_{\text{exp}}/\pi_{\text{num}} = 1.22/1.09$ ; kagome lattice:  $\pi_{\text{exp}}/\pi_{\text{num}} = 0.723/0.564$ ).

where the ratio of the elasto-active and reorientation lengths,  $\pi = l_e/l_r$ , which we refer to as the elasto-active feedback, is the unique control parameter.  $\hat{\mathbf{n}}_i$ 's are the polarization unit vectors,  $\mathbf{u}_i$  is the displacement field with respect to the reference configuration and  $\mathbb{M}$  is the dynamical matrix (Supplementary Information section 3.1).

The dynamics are best described when projected on the normal modes of the elastic structure sorted by order of growing energies. The dynamics condense mostly on two modes (Fig. 2-a,b), and describe a limit cycle driven by the misalignment of the polarity and the displacements (Fig. 2-c). In the case of the triangular lattice, the selected modes are the two lowest energy ones. Interestingly, in the case of the kagome lattice, these are the fourth and fifth modes, not the lowest energy ones. For both lattices, the selected pair of degenerated modes are strongly polarized along one spatial direction; they are extended and the polarization of the modes in each pair are locally quasi-orthogonal (Fig. 2-b). The numerical simulations confirm the experimental observations and allow for the observation of additional peaks in the spectrum, which belong to the same symmetry class as the two most actuated modes (Fig. 2-a,b, Supplementary Information section 6). As we shall see below these properties are at the root of the selection principle of the actuated modes.

The transition to the collective actuation regime (Fig. 3-a,b) is controlled by the elasto-active feedback. The larger it is, the more the particles reorient upon elastic deformations. Below a first threshold  $\pi_{FD}$ , the active solid freezes in a disordered state, with random polarizations and angular diffusion (Movies 4,7). Beyond a

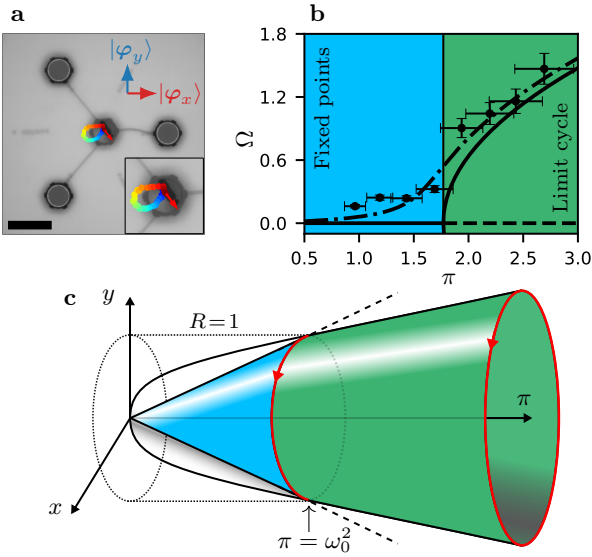


**FIG. 4. Single active unit dynamics.** **a**, One active unit connected to the three static vertices of a regular triangle (red arrow: polarity  $\hat{\mathbf{n}}$ ; trajectories color coded from blue to red by increasing time; scale bar: 10 cm). Inset: zoom on the active unit. **b**, Average rotation frequency  $\Omega$  as a function of  $\pi$ ; as measured ( $\bullet$ ), compared to the analytical expression of Eq.(2) (continuous line) and its correction in the presence of a constant bias (dot-dashed line).  $\pi_c^{\min} = \pi_c^{\max} = \pi_{FD} = \pi_{CA} = 1.77$ . **c**, Phase space structure of the displacements: for  $\pi < \omega_0^2$  an infinite set of marginal fixed points forms a circle of radius  $R = \pi/\omega_0^2$ ; for  $\pi > \omega_0^2$ , all such fixed points are unstable and a limit cycle of radius  $R = (\pi/\omega_0^2)^{1/2}$  branches off continuously.

second threshold  $\pi_{CA}$ , collective actuation sets in: homogeneous rotation takes place and the noiseless dynamics follow a limit cycle, composed of several frequencies in rational ratio (Supplementary Information, section 9.2). In between, the system is heterogeneous (Fig. 3-c and Movie 8), with the oscillating dynamics being favored close to the central node, while the frozen disordered regime invades the system layer by layer, from the pinned edges towards the center, as  $\pi$  decreases (Movie 11).

Altogether our experimental and numerical findings demonstrate the existence of a selective and collective actuation in active solids. This new kind of collective behaviour specifically takes place because of the elasto-active feedback, that is the reorientation of the active units by the displacement fields. The salient features of collective actuation are three-fold: (i) the transition from the disordered phase leads to a chiral phase with spontaneously broken symmetry; (ii) the actuated dynamics are not of inertial origin and take place on a few modes, not always the lowest energy ones, and therefore obey non-trivial selection rules; (iii) the transition follows a coexistence scenario made of successive deactuation steps. In the remainder of the paper, we unveil the physical origins of these three attributes.

The nature of the transition towards the chiral phase is best understood from considering the dynamics of a single particle (Fig. 4-a,b and Movies 9 and 10), which exhibits a transition to collective actuation in its sim-

plest form: the transition is continuous and only involves two degenerated and orthogonal normal modes. The dynamics can be solved analytically (Supplementary Information section 5). One predicts a continuous pitchfork bifurcation for the frequency, from the frozen disordered regime to the collective actuation one. The oscillation frequency is given by

$$\Omega = \omega_0 \sqrt{\pi - \pi_c}, \quad (2)$$

where  $\omega_0$  is the eigenfrequency of the degenerate modes, and  $\pi_c = \omega_0^2$  is the critical elasto-active feedback. Below  $\pi_c$ , the phase space structure for the displacements is composed of an infinite set of marginal fixed points, organized along a circle of radius  $R = \pi/\omega_0^2$ . At  $\pi_c$ , all such fixed points become unstable and a limit cycle of radius  $R = (\pi/\omega_0^2)^{1/2}$  branches off continuously (Fig. 4-c). Note that the oscillations result from the rotational symmetry of the polarity, and not from a Hopf bifurcation characterized by the onset of conjugated complex eigenvalues in the linearized dynamics.

Understanding how the nonlinear coupling of  $N$  such elementary units leads to the selection mechanism of the actuated modes requires a more involved analysis. One sees from Eqs. (1) that any configuration  $(\{\hat{\mathbf{n}}_i\}, \{\mathbf{u}_i = \pi \mathbb{M}_{ij}^{-1} \hat{\mathbf{n}}_j\})$  is a fixed point of the dynamics. In contrast with the one particle case, the linear destabilization threshold  $\pi_c(\{\hat{\mathbf{n}}_i\})$  depends on the fixed point configuration (Supplementary Information section 4.4). These thresholds are bounded  $\pi_c^{\min} \leq \pi_c(\{\hat{\mathbf{n}}_i\}) \leq \pi_c^{\max}$ . A first fixed point becomes unstable for  $\pi = \pi_c^{\min} = \omega_{\min}^2$ , where  $\omega_{\min}^2$  is the smallest eigenvalue of the dynamical matrix  $\mathbb{M}$  (Supplementary Information section 4.5) and an upper bound for  $\pi_c^{\max}$  (Supplementary Information section 4.6) reads :

$$\pi^{\text{upp}} = \min_{\{i,j\}} \left( \frac{\omega_i^2 + \omega_j^2}{c(|\varphi_i\rangle, |\varphi_j\rangle)} \right), \quad (3)$$

The function  $c(\bullet, \bullet)$  only depends on the eigenvectors of  $\mathbb{M}$ ,  $\{|\varphi_i\rangle\}$ . It is bounded between 0 and 1 and is maximal when the modes  $|\varphi_i\rangle$  and  $|\varphi_j\rangle$  are extended and locally orthogonal. More specifically, the pair of modes which dominates the dynamics,  $\{|\varphi_1\rangle, |\varphi_2\rangle\}$  for the triangular and  $\{|\varphi_4\rangle, |\varphi_5\rangle\}$  for the kagome lattice, are precisely the ones that optimize the bound. The construction of this bound is very general. It demonstrates that for any stable elastic structure, there is a strength of the elasto-active feedback above which the frozen dynamics is unstable and a dynamical regime must set in. It also captures the mode selection in the strongly condensed regime. Our findings about the linear stability of the fixed points for the triangular and kagome lattices are summarized in Extended Data Fig.1.

That some fixed points loose stability does not imply that collective actuation sets in: from these fixed points, the system can either slide to a neighboring stable fixed point or condense on some dynamical attractor. An exact theory to describe this condensation process is still missing in the general case, but can be formulated in the simpler, yet rich enough, case of a linear chain of  $N$  active particles, fixed at both ends. In the zero rest length

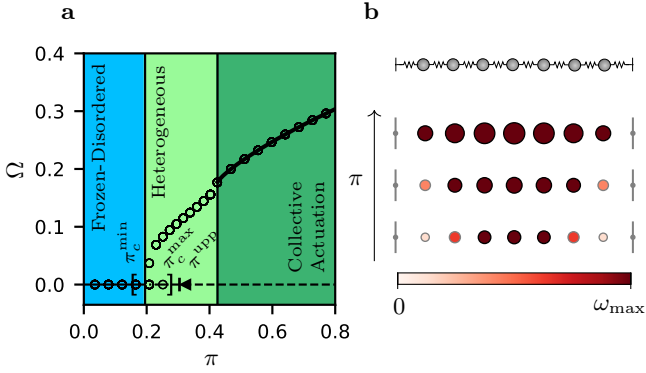


**FIG. 5. Collective actuation in a zero rest length chain of  $N$  nodes, pinned at both ends.** **a** Average oscillation frequency  $\Omega$  as a function of  $\pi$  for  $N = 7$  (continuous line: limit cycle found analytically; horizontal lines ( $\Omega = 0$ ): range of existence of only stable (continuous), only unstable (dashed) and coexisting stable and unstable (dot-dashed) fixed points; open circles: numerical data; same background color as for Fig. 3).  $\pi_c^{\min} = 0.152$ ,  $\pi_c^{\max} = 0.280$ ,  $\pi_c^{\text{upp}} = 0.304$ ,  $\pi_{FD} = 0.195$ ,  $\pi_{CA} = 0.426$ . **(b)**, Individual oscillation frequencies  $\omega_i$  for increasing values of  $\pi = [0.20, 0.33, 1.0]$ , in the  $N = 7$  chain. Radii of the symbols code for the average trajectory radius. Black, respectively gray, contours indicate  $R_i \geq 1$  and  $R_i \leq 1$ .

limit of the springs, the rotational invariance of the dynamical equations ensures that the eigenvalues and eigenvectors of the dynamical matrix are degenerated by pairs of locally orthogonal modes. In such a situation, the limit cycle solution, corresponding to the collective actuation regime, is found analytically (Supplementary Information, section 8.2), leading to a precise transition diagram, illustrated here for  $N = 7$  (Fig. 5a). When  $\pi$  exceeds the threshold value  $\pi_{CA}$ , the limit cycle is stable. If  $\pi_{CA} \leq \pi \leq \pi_c^{\max}$ , it coexists with an infinite number of stable fixed points. The evolution of their respective basins of attraction can be largely understood by studying the  $N = 2$  case (Supplementary Information section 8.3.1 Fig. S9). For  $\pi < \pi_{CA}$ , the dynamics leave the limit cycle and become heterogeneous.

The physical origin of the spatial coexistence lies in the normalization constraint of the polarity field,  $\|\hat{n}_i\| = 1$ , which translates into a strong constraint over the radii of rotation, namely  $R_i \geq 1$  (Supplementary Information, section 8.2.3 and 8.2.4). Whenever  $R_i$  becomes unity the polarity and displacement vectors become parallel, freezing the dynamics. The spatial distribution of the  $R_i$  is set by that of the modes selected by the collective actuation, with particles closer to the boundaries having typically a smaller radius of rotation than the ones at the center. The threshold value  $\pi_{CA}$ , below which the dynamics leave the limit cycle, is precisely met when the particles at the boundary reach a radius of rotation  $R = 1$ . For  $\pi < \pi_{CA}$ , the competition between outer particles, which want to freeze, and the central particles, which want to cycle, leads to the sequential layer by layer de-actuation, illustrated in Fig. 5b for a linear chain with  $N = 7$  and observed experimentally. The threshold value  $\pi_{FD}$  is reached when, eventually, the remaining particles at the center freeze and the system

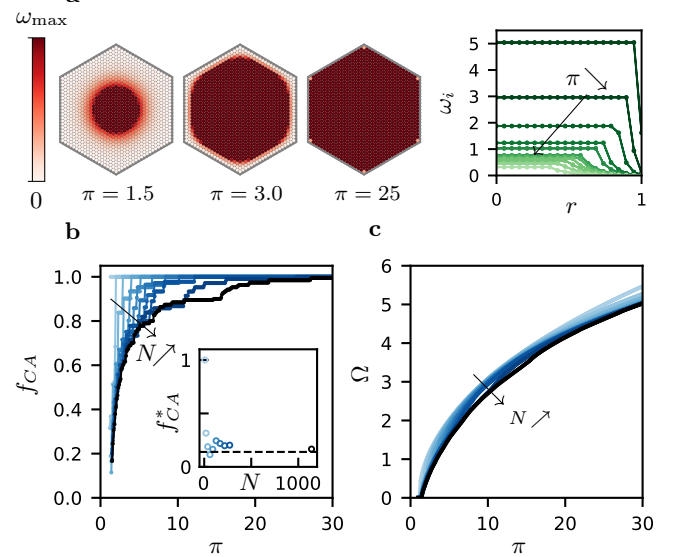


**FIG. 6. Large  $N$  triangular lattices.** **a** Spatial and radial variation of the individual oscillation frequencies  $\omega_i$ , for  $\pi \in [1.5, 1.6, 1.7, 1.8, 1.9, 2.0, 2.5, 3.0, 5.0, 10, 30]$ , in the case  $N = 1141$ , color coded from light to dark green. **b** Collective actuation fraction  $f_{CA}$  as a function of  $\pi$  for increasing  $N$  (Inset:  $f_{CA}$  at onset of collective actuation saturates to a finite value at large  $N$ ). **c** Collective oscillation frequency  $\Omega$  as a function of  $\pi$  for increasing  $N$ .  $N = 7, 19, 37, 61, 91, 127, 169, 217, 271, 631, 1141$ , color coded from light to dark blue.

discontinuously falls into the frozen disordered state.

The above analysis provides the theoretical grounds for all our experimental observations and gives our model the credit needed to investigate numerically the effect of the system size and the role of the noise.

Preliminary simulations with increasing values of  $N$ , while keeping the physical size  $L$  constant (Methods), indicate that collective actuation subsists for large  $N$ . The successive de-actuation steps converge toward a regular variation of both the fraction of nodes activated in the center of the system,  $f_{CA}$ , and the collective oscillation frequency,  $\Omega$  (Fig. 6 and Movie 12). At the transition to the frozen disordered state, when  $\pi = \pi_{FD}$ , the fraction of actuated nodes drops discontinuously to zero, from a finite value  $f_{CA}^*$ , which decreases with  $N$ , but saturates at large  $N$  (Fig. 6b). On the contrary the collective oscillation frequency  $\Omega$  decreases continuously to zero (Fig. 6c). The condensation level remains large, with a condensation fraction close to 60% for a wide range of values of  $\pi$  (Extended Data, Fig. 2). These results offer promising perspectives for the extension of our work to colloidal science and material design in general.

The role of noise, which was not considered in the numerical and theoretical analysis, is another matter of interest. In the frozen disordered regime, the noise is responsible for the angular diffusion of the polarities amongst the fixed points. In the collective actuation the noise level present in the experiment does not alter significantly the dynamics. Numerical simulations confirm that there is a sharp transition at a finite noise

amplitude  $D_c$ , below which collective actuation is sustained (Extended Data Fig.3-a). For noise amplitude much lower than  $D_c$ , the noise merely reduces the mean angular frequency  $\Omega$  (Extended Data Fig.3-b). Closer to the transition, the noise allows for stochastic inversions of the direction of rotation, restoring the chiral symmetry. (Extended Data Fig.3-c).

Finally, it has been shown very recently, that non reciprocal interactions, which are made possible in active systems, generically lead to chiral phases<sup>41</sup>, via a peculiar type of bifurcation, called exceptional points bifurcation. Here the individual polarity and displacement vectors do experience a non reciprocal interaction (Methods). It is therefore likely that the associated macroscopic fields are also coupled non-reciprocally. If this is confirmed by a proper coarse-graining procedure, it calls for the investigation of the disordered to chiral phase transition in active solids, which has not been addressed theoretically yet. In the same vein, one may ask whether the coarse-grained system shall obey standard or odd elasticity<sup>13</sup>.

More generally, the recent miniaturization of autonomous active units<sup>42</sup> opens the path towards the extension of our design principle to the scale of material science. In this context, extending the relation between the structural design of active materials – including the geometry and topology of the lattice, the presence of disorder, the inclusion of doping agents – and their spontaneous actuation offers a wide range of perspectives.

## References

1. Koenderink, G. H. *et al.* An active biopolymer network controlled by molecular motors. *Proc. Natl Acad. Sci.* **106**, 15192–15197 (2009).
2. Henkes, S., Fily, Y. & Marchetti, M. C. Active jamming: Self-propelled soft particles at high density. *Phys. Rev. E* **84**, 040301 (2011).
3. Menzel, A. M. & Löwen, H. Traveling and Resting Crystals in Active Systems. *Phys. Rev. Lett.* **110**, 055702 (2013).
4. Berthier, L. & Kurchan, J. Non-equilibrium glass transitions in driven and active matter. *Nat. Phys.* **9**, 310–314 (2013).
5. Ferrante, E., Turgut, A. E., Dorigo, M. & Huepe, C. Elasticity-based mechanism for the collective motion of self-propelled particles with springlike interactions: a model system for natural and artificial swarms. *Phys. Rev. Lett.* **111**, 268302 (2013).
6. Prost, J., Jülicher, F. & Joanny, J.-F. Active gel physics. *Nat. Phys.* **11**, 111–117 (Feb. 2015).
7. Ronceray, P., Broedersz, C. P. & Lenz, M. Fiber networks amplify active stress. *Proc. Natl Acad. Sci.* **113**, 2827–2832 (2016).
8. Woodhouse, F. G., Ronellenfitsch, H. & Dunkel, J. Autonomous actuation of zero modes in mechanical networks far from equilibrium. *Phys. Rev. Lett.* **121**, 178001 (2018).
9. Briand, G., Schindler, M. & Dauchot, O. Spontaneously flowing crystal of self-propelled particles. *Phys. Rev. Lett.* **120**, 208001 (2018).
10. Giavazzi, F. *et al.* Flocking transitions in confluent tissues. *Soft Matter* **14**, 3471–3477 (2018).
11. Klongvessa, N., Ginot, F., Ybert, C., Cottin-Bizonne, C. & Leocmach, M. Active glass: Ergodicity breaking dramatically affects response to self-propulsion. *Phys. Rev. Lett.* **123**, 248004 (2019).
12. Maitra, A. & Ramaswamy, S. Oriented active solids. *Phys. Rev. Lett.* **123**, 238001 (2019).
13. Scheibner, C. *et al.* Odd elasticity. *Nat. Phys.* **16**, 475–480 (2020).
14. Abercrombie, M. & Heaysman, J. E. Observations on the social behaviour of cells in tissue culture: II.“Monolayering” of fibroblasts. *Experimental cell research* **6**, 293–306 (1954).
15. Vilfan, A. & Frey, E. Oscillations in molecular motor assemblies. *Journal of physics: Condensed matter* **17**, S3901 (2005).
16. Szabo, B. *et al.* Phase transition in the collective migration of tissue cells: experiment and model. *Phys. Rev. E* **74**, 061908 (2006).
17. Mizuno, D., Tardin, C., Schmidt, C. F. & MacKintosh, F. C. Nonequilibrium mechanics of active cytoskeletal networks. *Science* **315**, 370–373 (2007).
18. Banerjee, S., Utuje, K. J. & Marchetti, M. C. Propagating stress waves during epithelial expansion. *Phys. Rev. Lett.* **114**, 228101 (2015).
19. Smeets, B. *et al.* Emergent structures and dynamics of cell colonies by contact inhibition of locomotion. *Proceedings of the National Academy of Sciences* **113**, 14621–14626 (2016).
20. Bi, D., Yang, X., Marchetti, M. C. & Manning, M. L. Motility-driven glass and jamming transitions in biological tissues. *Phys. Rev. X* **6**, 021011 (2016).
21. Chen, C., Liu, S., Shi, X.-q., Chaté, H. & Wu, Y. Weak synchronization and large-scale collective oscillation in dense bacterial suspensions. *Nature* **542**, 210–214 (2017).
22. Needelman, D. & Dogic, Z. Active matter at the interface between materials science and cell biology. *Nat. Rev. Mater.* **2**, 1–14 (2017).
23. Holmes, D. F. *et al.* Synchronized mechanical oscillations at the cell–matrix interface in the formation of tensile tissue. *Proc. Natl Acad. Sci.* **115**, E9288–E9297 (2018).
24. Peyret, G. *et al.* Sustained oscillations of epithelial cell sheets. *Biophys. J.* **117**, 464–478 (2019).
25. Henkes, S., Kostanjevec, K., Collinson, J. M., Sknepnek, R. & Bertin, E. Dense active matter model of motion patterns in confluent cell monolayers. *Nat. Commun.* **11**, 1–9 (2020).
26. Brandenbourger, M., Locsin, X., Lerner, E. & Coulais, C. Non-reciprocal robotic metamaterials. *Nat. Commun.* **10**, 1–8 (2019).
27. Brambilla, M., Ferrante, E., Birattari, M. & Dorigo, M. Swarm robotics: a review from the swarm engineering perspective. *Swarm Intell.* **7**, 1–41 (2013).
28. Pratissoli, F., Reina, A., Lopes, Y. K., Sabattini, L. & Groß, R. *A soft-bodied modular reconfigurable robotic system composed of interconnected Kilobots* in *MRS* (2019), 50–52.
29. Li, S. *et al.* Particle robotics based on statistical mechanics of loosely coupled components. *Nature* **567**, 361–365 (2019).
30. Dorigo, M., Theraulaz, G. & Trianni, V. Reflections on the future of swarm robotics. *Sci. Robot.* **5** (2020).
31. Oliveri, G., van Laake, L. C., Carissimo, C., Miette, C. & Overvelde, J. T. Continuous learning of emergent behavior in robotic matter. *Proc. Natl Acad. Sci.* **118** (2021).
32. Bertoldi, K., Vitelli, V., Christensen, J. & Van Hecke, M. Flexible mechanical metamaterials. *Nature Reviews Materials* **2**, 1–11 (2017).
33. Pishvar, M. & Harne, R. L. Foundations for soft, smart matter by active mechanical metamaterials. *Adv. Sci.* **7**, 2001384 (2020).
34. Toner, J. & Tu, Y. Long-Range Order in a Two-Dimensional Dynamical XY Model: How Birds Fly Together. *Phys. Rev. Lett.* **75**, 4326–4329 (1995).
35. Vicsek, T. & Zafeiris, A. Collective motion. *Physics Reports* **517**, 71–140 (2012).

36. Bricard, A., Caussin, J.-B., Desreumaux, N., Dauchot, O. & Bartolo, D. Emergence of macroscopic directed motion in populations of motile colloids. *Nature* **503**, 95–98 (Oct. 2013).
37. Marchetti, M. C. *et al.* Hydrodynamics of soft active matter. *RMP* **85**, 1143 (2013).
38. Wittkowski, R. *et al.* Scalar  $\varphi$  4 field theory for active-particle phase separation. *Nat. Commun.* **5**, 1–9 (2014).
39. Peshkov, A., Bertin, E., Ginelli, F. & Chaté, H. Boltzmann-Ginzburg-Landau approach for continuous descriptions of generic Vicsek-like models. *Eur. Phys. J.: Spec. Top.* **223**, 1315–1344 (2014).
40. Dauchot, O. & Démery, V. Dynamics of a self-propelled particle in a harmonic trap. *Phys. Rev. Lett.* **122**, 068002 (2019).
41. Fruchart, M., Hanai, R., Littlewood, P. B. & Vitelli, V. Non-reciprocal phase transitions. *Nature* **592**, 363–369 (2021).
42. Miskin, M. Z. *et al.* Electronically integrated, mass-manufactured, microscopic robots. *Nature* **584**, 557–561 (2020).

**Supplementary Information** is available in the online version of the paper.

**Acknowledgements** We acknowledge financial support from Ecole Doctorale ED564 “Physique en Ile de France” for P.B.’s Ph.D. grant. D.S. was supported by a Chateaubriand fellowship.

**Author Contributions** O.D., C.C. and G.D. conceived the project. P.B. and D.S. performed the experiments. P.B., D.S., and O.D. analyzed the experimental results. P.B., V.D., O.D., C.H. and G.D. worked out the theory. All contributed to the writing of the manuscript.

**Author Institutions** <sup>1</sup>*Gulliver UMR CNRS 7083, ESPCI Paris, Université PSL, 75005 Paris, France.* <sup>2</sup>*School of Physics and Astronomy, Tel-Aviv University, Tel Aviv 69978, Israel.* <sup>3</sup>*Instituto de Física, Pontificia Universidad Católica de Chile, Casilla 306, Santiago, Chile.* <sup>4</sup>*ANID - Millennium Nucleus of Soft Smart Mechanical Metamaterials, Santiago, Chile.* <sup>5</sup>*Van der Waals-Zeeman Institute, Institute of Physics, Universiteit van Amsterdam, Science Park 904, 1098 XH Amsterdam, the Netherlands.* <sup>6</sup>*Univ Lyon, ENS de Lyon, Univ Claude Bernard Lyon 1, CNRS, Laboratoire de Physique, F-69342 Lyon, France.*